Optical Materials 38 (2014) 278–285

Contents lists available at ScienceDirect

Optical Materials

journal homepage: www.elsevier.com/locate/optmat

Structural phase analysis, band gap tuning and fluorescence properties of Co doped TiO_2 nanoparticles

Alamgir [a,b], Wasi Khan [b,*], Shabbir Ahmad [a], M. Mehedi Hassan [b], A.H. Naqvi [b]

[a] Department of Physics, Aligarh Muslim University, Aligarh 202002, India
[b] Centre of Excellence in Materials Science (Nanomaterials), Department of Applied Physics, Z.H. College of Engineering & Technology, Aligarh Muslim University, Aligarh 202002, India

ARTICLE INFO

Article history:
Received 6 July 2014
Received in revised form 20 October 2014
Accepted 23 October 2014
Available online 15 November 2014

Keywords:
Co doped TiO_2 nanoparticles
XRD & Raman spectroscopy
TEM
Band gap
Fluorescence properties

ABSTRACT

This paper reports on structural and optical properties of Co (0, 3, 5 & 7 mol%) doped TiO_2 (titania) nanoparticles (NPs) synthesized by employing acid modified sol–gel method. The crystalline phase of the pure and doped NPs was observed with X-ray diffraction (XRD) followed by Raman scattering technique. Field emission scanning electron microscope and transmission electron microscopy give the morphological details. Fourier transform infrared spectra indicate the bonding interactions of Co ions with the titania lattice framework. Optical studies were attained with UV–visible absorption and fluorescence emission spectroscopy. XRD analysis reveals that all prepared samples have pure anatase phase with tetragonal symmetry devoid of any other secondary phase. The average crystallite size of all samples was calculated using Scherrer's formula and was found to vary from 8 to 10 nm with doping concentration of Co. The Raman spectroscopy further confirmed the formation of TiO_2 in anatase structure in both pure and Co doped TiO_2 NPs. The most intense Raman active E_g peak of TiO_2 NPs shifted to higher energy on doping. Both UV–visible and fluorescence spectra show a blue shift in their absorption and band edge emission subsequently on increasing with Co percentage in titania host matrix, wherever there is an indication of quantum confinement effect with widening of band gap on decreasing in NPs size. There is also a possibility of strong Coulomb interaction effect on the optical processes involving the Co ions. However, the intensities of different emission spectra are not the same but decrease profoundly for doping samples due to concentration quenching effect.

1. Introduction

Scientific investigations on nanoparticles, nanocrystals, nanolayer thin films, quantum dots and quantum well, atomic and molecular clusters have grown dramatically over the past decade. A general approach in these fields is to study the optical properties of a given substance as a function of structure, size and dimensionality. When the characteristic size of the particles is comparable or smaller than its bulk Bohr exciton diameter, their optical properties become strongly dependent on size due to the quantum confinement of electrons and holes [1–5]. Recently, scholarly efforts seem to develop metal oxide semiconductor nanoparticles, which attracts a great deal of attention in terms of their potential applications in solar energy conversion and energy storage devices. Among these semiconductors, titanium dioxide is a wide band gap semiconductor and is believed to be one of the most promising known material for its high refractive index leading to a high hiding power, whiteness, resistance to photo corrosion, high dielectric constant, useful photo catalytic properties, chemical stability, low cost and non-toxicity [6–11]. These properties make this material a candidate for a large number of prime applications in many fields of chemical engineering and materials engineering including traditional catalysis or photo-catalysis, dye-sensitized solar cells, lithium insertion-based devices, integrated circuits, gas sensors, sunscreens, and in the paint industry [12]. More recently, Co doped TiO_2 generates a wide interest as diluted magnetic semiconductor (DMS) because of its ferromagnetic behaviour above room temperature for low Co doping concentration and it exhibits the Curie temperature, $T_C \sim 650$ K [13–15]. This feature makes it a promising candidate for fabricating various magneto-optical and spintronic devices.

The optical response as well as the room temperature ferromagnetism in Co doped anatase titania are affected by defect states and oxygen vacancies in the crystal lattice [16,17]. The analysis of luminescence spectrum is a cheap and effective way to study the electronic structure, optical and photochemical properties of semiconductor materials, through which the information such as

* Corresponding author. Tel./fax: +91 571 2700042.
E-mail address: wasiamu@gmail.com (W. Khan).

http://dx.doi.org/10.1016/j.optmat.2014.10.054
0925-3467/

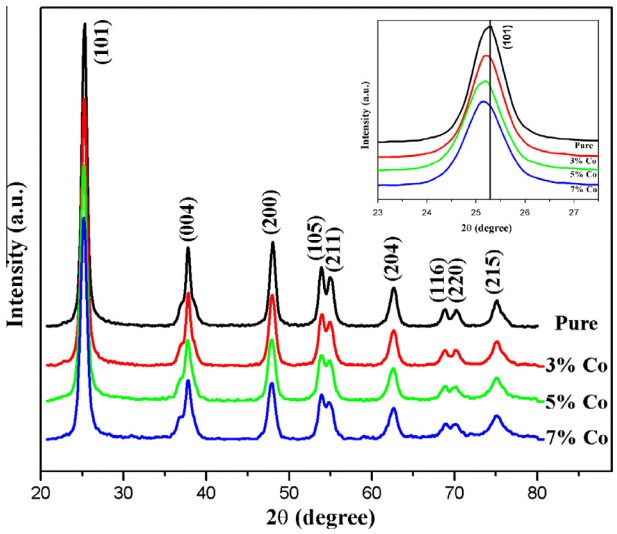

Fig. 1. XRD patterns of $Ti_{1-x}Co_xO_2$ (x = 0.00, 0.03, 0.05 and 0.07) NPs.

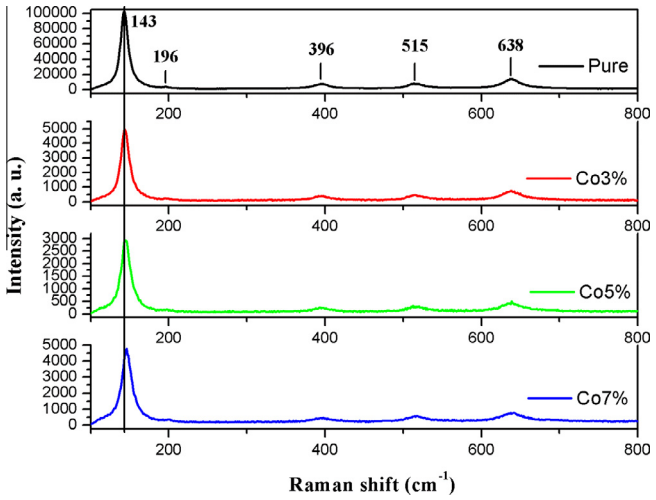

Fig. 2. Raman spectra of $Ti_{1-x}Co_xO_2$ (x = 0.00, 0.03, 0.05 and 0.07) NPs.

oxygen vacancies and defects, as well as the efficiency of charge carrier trapping can be understood [18,19].

Earlier investigations reported the microstructural, morphological, optical properties and luminescence performance of the transition metal doped TiO_2. Out of which luminescence performance appears to be extremely sensitive to the conditions employed during synthesis. There are hardly few papers reported on fluorescence properties of Co doped TiO_2 NPs. In the literature, it has been reported either on colloidal form of pure titania or recently few on nanocomposite forms. These factors motivated us to investigate systematically the microstructural and optical properties of Co doped TiO_2 NPs. In this communication, we have successfully synthesized nanocrystalline TiO_2 powder with low concentration of Co ions (0, 3, 5 and 7 mol%) doped by simple acid modified sol–gel method to investigate the effect of Co doping on above mentioned properties of purely anatase titania NPs. Here we have used glacial acetic acid in the conventional sol–gel method for preventing titanium (IV) isopropoxide to precipitate in water medium.

2. Experimental

2.1. Material and synthesis

NPs of Co doped TiO_2 with stoichiometric formula $Ti_{1-x}Co_xO_2$ (x = 0.00, 0.03, 0.05, and 0.07) were prepared by acid modified sol–gel route. All reagents used in the synthesis experiments were of analytical grade purchased from commercial sources and utilized without further purification. Titanium (IV) isopropoxide solution [$C_{12}H_{28}O_4$·Ti] and cobalt nitrate [$Co(NO_3)_2$·$6H_2O$] were purchased from Alfa Aesar. Glacial acetic acid (99.9%) was obtained from Thomas Baker and absolute ethanol (99.9%) AR-grade was from Changshu Yangyuan Chemical, China.

Stoichiometric amount of cobalt nitrate (the dopant starting material) was dissolved in 60 ml of deionized water at room temperature followed by an addition of 5 ml glacial acetic acid to obtain a solution say S-1. Stoichiometric amount of titanium (IV) isopropoxide was dissolved in 40 ml of absolute ethanol with constant stirring to form another solution say S-2. The solution S-2 was added drop-wise very slowly into the solution S-1 during 60 min under vigorous stirring. Subsequently, the obtained sol was stirred continuously for 2 h and was aged for 48 h at room temperature. As-prepared gel was dried for 12 h at 80 °C. The obtained solid was ground and calcined at 450 °C for 6 h (heating rate 2.5 °C/min, cooling rate 1.5 °C/min), then ground again and ready for characterizations.

2.2. Characterizations details

To confirm the formation of a single phase, X-ray diffraction (XRD) patterns of undoped and doped TiO_2 NPs were recorded with a Rigaku Miniflex-II X-ray diffractometer equipped with high intense Cu-K_α radiations (λ = 1.5406 Å) operated at a voltage of 30 kV and current 15 mA at scanning rate of 2°/min in 2θ ranging from 20° to 80°. For further confirmation of single phase, Raman spectra of all the samples were recorded at room temperature on Raman spectrometer (Renishaw, UK) with Ar ion laser of wavelength 514.5 nm and power 50 mW. Elemental compositions were known from energy dispersive X-ray spectroscopy (EDS) equipped with field emission scanning electron microscope (FESEM) from Bruker-NANO NOVA. Transmission electron microscope (TEM) micrographs and selected area electron diffraction (SAED) pattern of the prepared NPs were captured with JEOL, JEM-2010 Transmission electron microscope. The presence of different bonding vibrational frequencies were determined by a Perkin Elmer Fourier transform infrared (FTIR) spectrometer (Spectrum 2) using KBr pellets as medium. UV–visible and fluorescence emission spectra with

Table 1
Variation of crystallite size, lattice parameters and unit cell volume with doping concentration.

Co conc. (%)	Crystallite size (nm)	Lattice parameter		Unit cell volume (Å^3)	d value (Å) (1 0 1) plane
		$a = b$ (Å)	c (Å)		
0	10.5	3.78733(2)	9.50845(3)	136.38796(4)	3.51698
3	9.9	3.78855(7)	9.50825(9)	136.47297(9)	3.52996
5	8.9	3.78880(5)	9.50810(2)	136.48883(7)	3.53190
7	8.7	3.78910(7)	9.50802(2)	136.50929(7)	3.53599

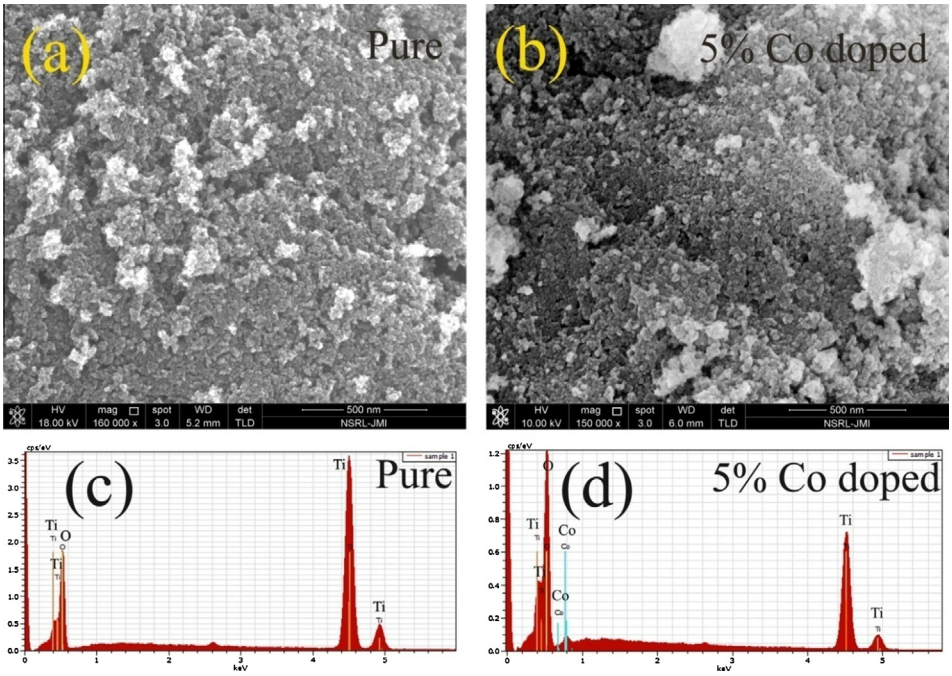

Fig. 3. SEM micrographs of (a) pure TiO_2 NPs and (b) 5% Co doped TiO_2 NPs, and EDS spectrum of (c) pure TiO_2 NPs and (d) 5% Co doped TiO_2 NPs.

excitation wavelength λ_{ext} = 275 nm were recorded with UV–visible spectrometer (Perkin Elmer-Lambda 35), and Fluorescence spectrometer (Perkin Elmer LS-55) respectively.

3. Results and discussion

3.1. X-ray diffraction (XRD) analysis

The XRD patterns of pure and Co doped TiO_2 NPs, calcined at 450 °C are shown in Fig. 1. XRD data were analyzed using PowderX software. For pure and Co doped TiO_2 NPs, the diffraction peaks occurring at 25.30°, 37.78°, 48.02°, 53.90°, 54.94°, 62.60°, 68.86°, 70.19° and 75.12° have been assigned to the lattice planes (101), (004), (200), (105), (211), (204), (116), (220), and (215) respectively. These lattice planes are attributed to the signals of pure tetragonal anatase phase of TiO_2 with a space group $I4_1/amd$ (JCPDS File No. 78-2486). Regardless of the concentration of the substituted Co into TiO_2 crystal lattice, there was no trace of any secondary phases such as rutile and brookite phase of TiO_2 or any Co-oxides phases and Co composites. It is known that tetragonal anatase TiO_2 is constructed from coordination Ti-6 (octahedral) and O-3 (trigonal planer). However, downshift of the (101) peak in samples with doping as shown in the inset of Fig. 1 is caused by a successive increase of the d value of the (101) plane in Co doped samples, indicating that larger Co cations have successfully assimilated into the anatase structure and substituted Ti^{4+} in the anatase TiO_2 lattice [20]. Because of different ionic charges of Ti^{4+} and Co ions (i.e. Co^{2+} and Co^{3+}), dopant substitutions lead to the creation of crystal defects and oxygen ion vacancy in order to neutralize the charge imbalance in titania structure. Due to the small size of the NPs, not all the added dopants undergo host lattice interior (i.e. octahedral position) rather some dopants may sit on the surfaces or some may on the grain boundaries, and they go beyond the detection limit of XRD. These few dopant atoms at the grain boundary disturb the periodicity of the lattice; inhibit crystal growth and crystallite size decreases. Hence, doped samples show lowering of peak intensity and an increase in full width at half maximum of XRD reflections. The average crystallite sizes for all the samples were calculated using Scherrer's formula [21] and tabulated in Table 1. It is clear evident from the XRD analysis that there is no change in structural symmetry (tetragonal) except the changes in lattice parameters. On increasing Co concentration, the increase in d value confirms elongation of the unit cell along *a*-axis while a slight decrease along *c*-axis when smaller sized Ti^{4+} (0.61 Å) is replaced by larger sized Co^{2+} (0.65 Å), resulted increase in the unit cell volume [20,22]. Earlier investigations and their XPS analysis show that the Co^{2+} ion occupy substitutional cation sites in the TiO_2 matrix [23–25]. These results are consistent with XRD data.

Table 2
Compositions of pure and 5 mol% Co doped TiO_2 NPs by EDS technique.

Sample	Elements	wt%	Error (wt%)
Pure TiO_2 NPs	Ti	43.94	1.52
	O	56.06	8.57
	Total	100	
Co doped TiO_2 NPs	Ti	53.64	2.08
	O	43.87	5.77
	Co	2.49	0.45
	Total	100	

3.2. Raman scattering studies

Raman spectroscopy is a sensitive, fast and nondestructive method. It is one of the most effective tools for the study of crystallinity and defects structure associated with the materials. The change of Raman spectra is related to non-stoichiometry and phonon confinement effect in nanostructured materials [26–29]. Oxygen deficiency within the material, however, strongly affects the Raman spectrum by producing frequency shift and broadening of some spectral peaks. The crystallite size in the nanoscale range may affect the frequency shift and broadening of Raman peaks due to the phonon confinement [30,31]. The Raman signal of

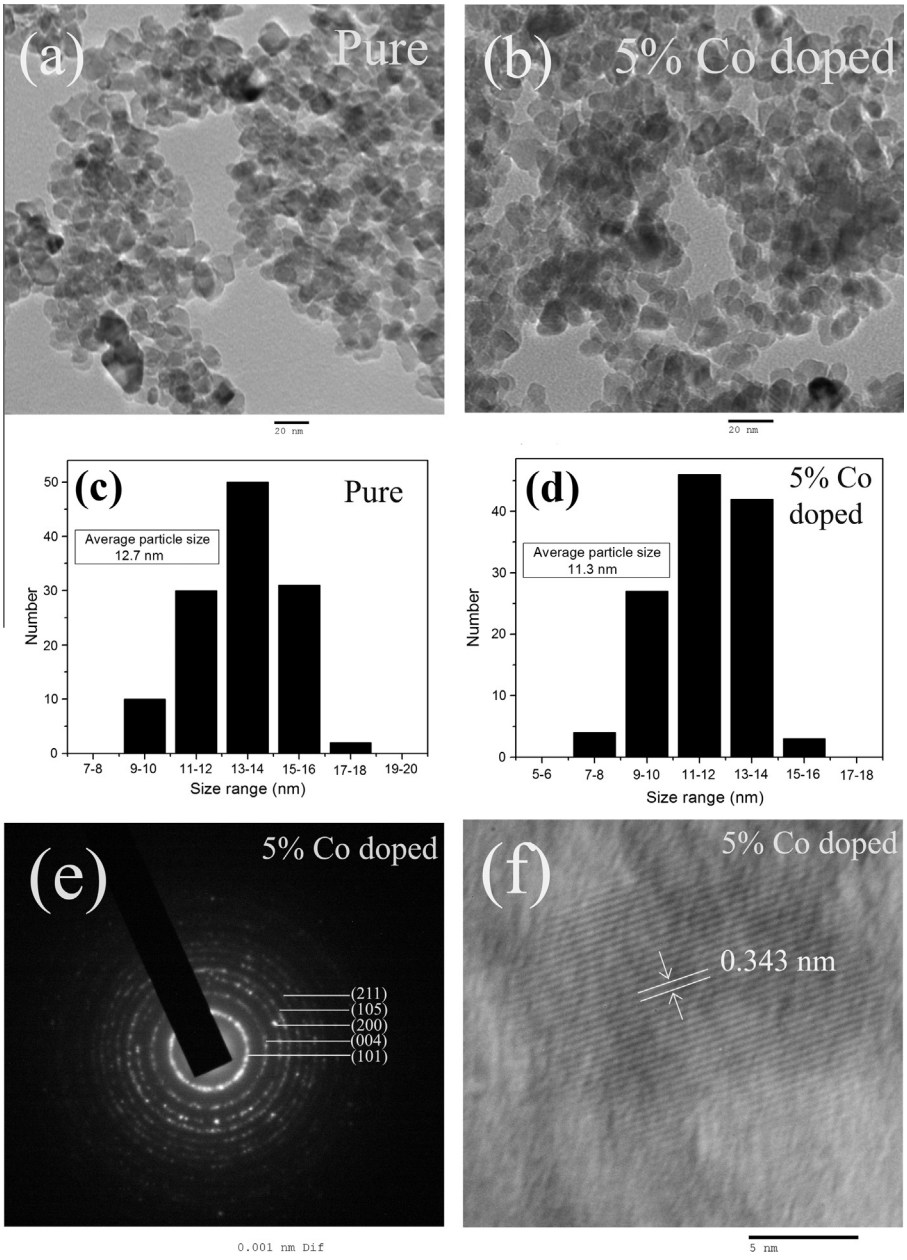

Fig. 4. TEM images of (a) pure, (b) 5% Co doped TiO_2 NPs, histograms of (c) pure, (d) 5% Co doped TiO_2 NPs, (e) SAED pattern of 5% Co TiO_2 NPs, and (f) HRTEM image of 5% Co doped TiO_2 NPs.

TiO_2 is very sensitive to the vibrational mode of oxygen ions in the Ti–O bond. The strength of the Raman signal depends upon the polarizability of oxygen ions surrounding Ti^{4+} in the basic TiO_6 octahedral [32]. Presence of oxygen vacancies will affect the vibration of Ti–O bond and the direct consequence of these vacancies can be revealed in the intensity, position, and width of the Raman signal.

The pure and Co doped titania NPs were characterized by micro-Raman spectroscopy as shown in Fig. 2 and it gave complimentary phase analysis. The group-theoretical analysis gives that TiO_2 anatase phase contains six Raman active modes ($A_{1g} + 2B_{1g} + 3E_g$), three infrared (IR) active modes (A_{2u} and $2E_u$) and a silent B_{2u} mode. In this section of this communication, we are dealing with only Raman active modes. The Raman spectra of single crystals anatase phase were investigated by Ohsaka [33] who concluded that six allowed modes appear at 144 cm^{-1} (E_g), 197 cm^{-1} (E_g), 399 cm^{-1} (B_{1g}), 513 cm^{-1} (A_{1g}), 519 cm^{-1} (B_{1g}) and 639 cm^{-1} (E_g). In Fig. 2, it has been observed that NPs have three E_g modes, appeared at 143 cm^{-1}, 196 cm^{-1} and 638 cm^{-1} whereas one B_{1g} mode has appeared at 396 cm^{-1} and another B_{1g} mode has overlapped with A_{1g} at 515 cm^{-1} as they are very close to each other. It is reported that Raman band of anatase TiO_2 occurring at 516 cm^{-1} at room temperature is split into two peaks centered at 513 (A_{1g}) and 519 cm^{-1} (B_{1g}) [34]. In the present Raman spectra, the absence of the Raman active modes at 612, 447 (intense line) and 235 cm^{-1} which correspond to the rutile phase of titania, reconfirms the anatase phase purity of synthesized pure and doped samples. No bands are observed for oxides of cobalt, which also supports the presence of dopant cation in the substitutional positions of the titania host lattice for Co doped NPs. However, the most intense E_g Raman mode appeared at 143 cm^{-1} shows consistent blue shift with increasing of Co doping;

this is also consistent with XRD result. With the increasing of doping concentration, the defects increase and the crystallite size decreases, and gradually the E_g peak shifts towards higher energy. Moreover, for doped samples, all observed peaks are broadened and intensities are decreased gradually with increase in Co concentration up to 5 mol%, afterward intensities enhanced for 7 mol% Co doped sample. This may be due to approaching the limit of Co solubility in the matrix or maybe there is an enhancement of Raman peak [23,34].

3.3. FESEM and EDS analysis

The morphologies of pure and Co (5%) doped TiO_2 NPs were analyzed by FESEM as displayed in Fig. 3(a) and (b) respectively. The images show that particles are somewhat spherical in nature. Nevertheless, most of them are in agglomerated form. To reinforce the assumption that the dopant element is homogeneously distributed in substitutional sites of the anatase structure, samples of pure TiO_2 and Co (5%) doped TiO_2 were enlightened with EDS analysis and compared. The EDS patterns for pure and Co (5%) doped TiO_2 NPs are shown in Fig. 3(c) and (d) respectively, whereas the compositional analysis is tabulated in Table 2. The EDS data endorse that the samples are composed of Co, Ti and oxygen. EDS analysis shows that there is desired composition of cobalt with respect to titanium center in the doped sample and cobalt doping leads to the oxygen deficiencies.

3.4. TEM with SAED analysis

Complementary morphological clarification can be attained through the TEM with the SAED study. TEM images in Fig. 4(a) and (b) respectively reveal that pure and 5% cobalt doped TiO_2 NPs were agglomerated and non-spherical in shapes; and the size distribution of them is shown in histograms Fig. 4(c) and (d). It is clear from the histograms that there is a little contraction in average particle size for 5% cobalt doped sample. It is clear evident from these micrographs that synthesized titania samples have small size but they are well crystalline in nature. The TEM results are in concord with XRD data calculated using Scherrer's formula. TEM investigations give the evidence of no segregated secondary phases of cobalt oxides and support homogeneous substitution of cobalt in the titania matrix. The HRTEM study was further executed to analyze the lattice fringes for the 5% doped NPs, which are presented in the inset of Fig. 4(f). The clear lattice fringes obtained with an interval of 0.343 nm imply that the NPs are highly crystalline and give the d value ~0.343 nm which is in correlation with the d value obtained from XRD data. It corresponds to (101) anatase planes as shown in Fig. 1 and tabulated in Table 1. The crystalline nature is further analyzed from selected area electron diffraction (SAED) pattern displayed in Fig. 4(e) where the ring pattern indicates polycrystalline anatase nature of TiO_2 NPs. The electron diffraction image demonstrates that ring consists of well distinct spots due to the high crystallinity of titania indicated as anatase phase with major (101) planes. This is in well concord with the XRD pattern.

3.5. FTIR analysis

FTIR spectra of $Ti_{1-x}Co_xO_2$ (x = 0.00, 0.03, 0.05 and 0.07) NPs at room temperature have been recorded in order to study the vibrational bands present in the system as projected in Fig. 5. Generally, the FTIR spectra give information about functional groups present in a system, the molecular geometry, and inter or intra-molecular interactions.

A large broad absorption peak at ~3150 cm^{-1} is attributed to the –OH (hydroxyl) group. This band corresponds to the O–H stretching vibration of the Ti–OH group on the surface [35]. The peak around ~2340 cm^{-1} is due to stretching mode of CO_2 molecule, being tapped with the titina nanoparticles [36]. The sharp band found at 1590 cm^{-1} is due to the H–O–H bending of physically absorbed water [37], indicating the existence of water absorbed on the surface of nanocrystalline titina powders. In the low energy region below 1000 cm^{-1}, a very strong absorption at 770 cm^{-1} has been observed, which is the characteristic peak of anatase titania due to Ti–O bond [38]. A small hump can be identified around 500 cm^{-1} as the Ti–O–Ti stretching vibration in TiO_2 network. These bonds are important due to their relation to the photocatalytic activity. The small hump shifts to the higher wavenumbers, observed in Fig. 5, may be due to decrease in size of the nanoparticles or may be due to asymmetric stretching with the formation of Ti–O–Co band [38] with increasing in Co concentration from 0 to 3, 5 and 7 mol% respectively. There is no band around ~1389 cm^{-1} due to the bending vibrations of the C–H bond in all the synthesized samples [39]. In addition, there are no excess bands assigned to the alkoxy groups. Therefore, addition of glacial acetic acid did not cause any residues on pure and doped titania NPs surfaces after calcinations.

3.6. UV–visible spectroscopy

Absorption and fluorescence spectroscopies are powerful non-destructive techniques to explore the optical properties of semiconducting nanoparticles. The optical properties of semiconductors are generally determined by its electronic structure, so the essence of light absorption will be found through investigating the relationship between electronic structure and optical properties of titania. We have explored the optical properties and analyzed the energy band gap of pure and Co doped TiO_2 NPs by UV–visible absorption spectroscopy as shown in Fig. 6. The absorbance can vary depending upon some factors like particle size, oxygen deficiency, defects in material prepared, etc. [40]. In order to calculate the direct band gap (E_g), we have taken the help of Tauc's relation

$$\alpha h\nu = A(h\nu - E_g)^n \quad (1)$$

where α is the absorption coefficient, A is a constant and $n = 1/2$ for direct or $n = 2$ for indirect allowed transitions of the semiconductors. An extrapolation of the linear region to $\alpha = 0$ of a plot of $(\alpha h\nu)^2$ versus $h\nu$ gives the value of the optical band gap E_g. Direct

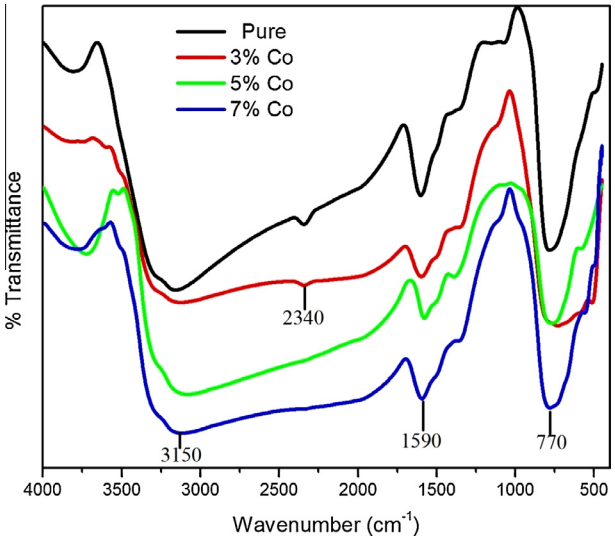

Fig. 5. FTIR spectra of $Ti_{1-x}Co_xO_2$ (x = 0.00, 0.03, 0.05 and 0.07) NPs recorded at room temperature.

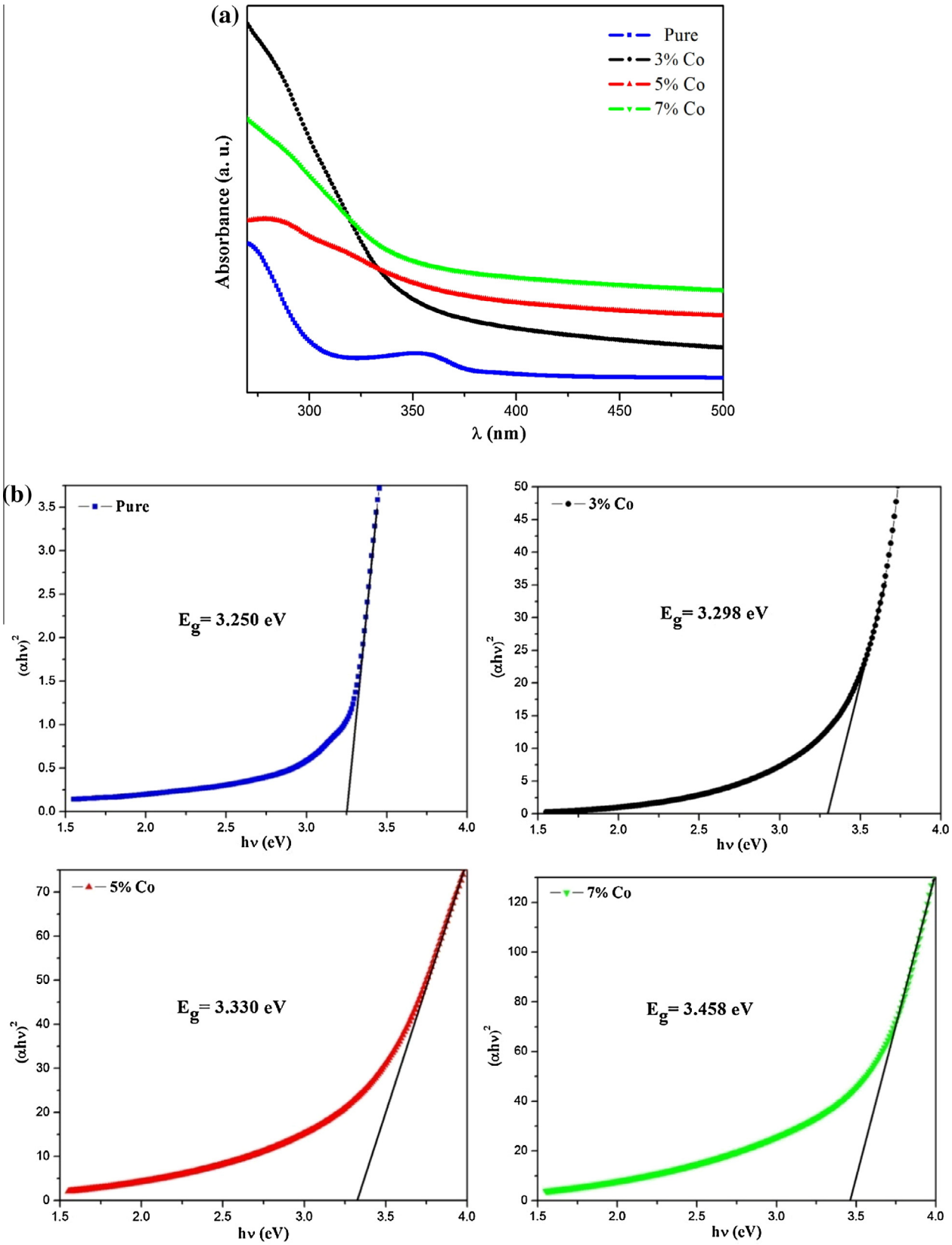

Fig. 6. (a) UV–visible absorption spectra and (b) optical band gap determination of $Ti_{1-x}Co_xO_2$ (x = 0.00, 0.03, 0.05 and 0.07) NPs.

band gaps of synthesized $Ti_{1-x}Co_xO_2$ (x = 0.00, 0.03, 0.05 and 0.07) NPs are found to be 3.250 eV, 3.298 eV, 3.330 eV, and 3.458 eV respectively. The literature reports the value 3.23 eV for pure anatase phase titania [41]. Fig. 6 shows a blue shift of absorption and increase in band gap. This kind of blue shift in absorption spectra observed in literature with the decrease in particle size has been reported earlier and can be attributed to the well-known quantum size effect for semiconductors for the titania particle size below

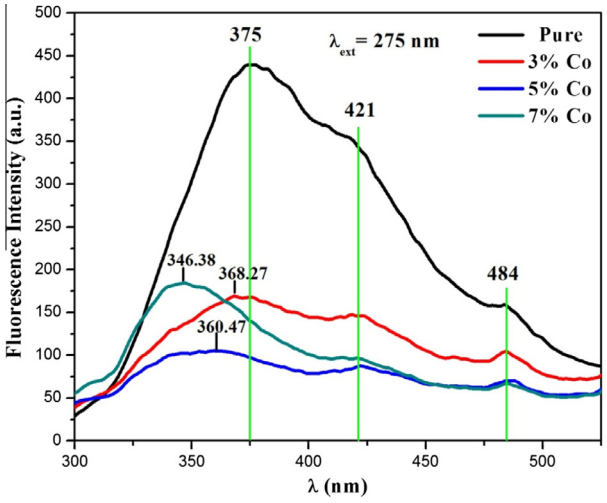

Fig. 7. Fluorescence emission spectra of $Ti_{1-x}Co_xO_2$ (x = 0.00, 0.03, 0.05 and 0.07) NPs with excitation wavelength λ_{ext} = 275 nm.

10 nm [42]. It may also be due to strong Coulomb interaction effect on the optical processes involving the Co ions due to limited solubility in titania host matrix [43].

3.7. Fluorescence study

We have also recorded the fluorescence spectra of the $Ti_{1-x}Co_xO_2$ (x = 0.00, 0.03, 0.05 and 0.07) NPs at room temperature. Fig. 7 contains the photo-induced fluorescence spectra of all samples for an excitation source of wavelength of 275 nm. From the UV-absorption spectrum in Fig. 6, it is clear that the wavelength around 275 nm sweetens well for exciting these samples. After excitation by photon, the electron–hole pairs recombine in various processes. The recombination rate is closely related to the electronic structure and crystal structure. The curves show three emission peaks - one centered around UV region at 375 nm, another two in the visible region at 421 nm and 484 nm for the pure one. However, for the doping samples, the peak in UV region gradually shifts towards the lower wavelength whereas the other two in the visible region remain almost intact. The strong UV emission peaks at 375 nm for the pure sample and at lower wavelengths for the doped titania NPs are due to band gap transition or the band edge emission of the host TiO_2 [44,45]. These shifts of the emission peaks on Co doping indicate the widening of optical band gap of titania NPs and may be associated to the strong Coulomb interaction effect which induces blue shift as solubility of Co is limited in titania host lattice [44]. However, we cannot completely rule out the contribution of quantum size effects for this blue shift. The emission peaks at 421 nm and 484 nm lying beyond 400 nm are associated with self-trapped excitons, oxygen vacancies, surface defects, etc. [46]. The 421 nm peak can be ascribed as self-trapped excitons localized on TiO_6 octahedra and the peak at 484 is attributed to the defect centers associated with oxygen vacancies [45]. Incorporation of Co ions in TiO_2 also reduces the emission peak intensities considerably for all the doped samples by forming large number of nonradiative centers, which act as luminescence quencher [45].

4. Conclusion

In summary, we have successfully synthesized (0, 3, 5 and 7 mol%) Co doped TiO_2 NPs through acid modified sol–gel method. XRD results show that the particles are pure tetragonal anatase phase structure with size 8–10 nm, and the grain size can be controlled with doping concentration. XRD and HRTEM analysis confirm the absence of any secondary phase other than the anatase TiO_2 whereas Raman analysis gives the further compliment to the formation of the phase of the products. EDS result confirms the existence of the cobalt in the TiO_2 nanomaterials and shows oxygen vacancies in doped titania. Raman spectra reveal that the characteristic intense band of tetragonal anatase TiO_2 at 143 cm^{-1} exhibits a decrease in intensity up to 5 mol% and then enhanced for 7 mol% Co doping. This Raman active E_g peak of TiO_2 NPs shifts to higher energy on doping and this result is also in good agreement with particle size calculation. This may be due to oxygen vacancy that affects the Ti–O bond and causes shifting and broadening of peak. The coordination of oxygen ions surrounding the Ti ion was confirmed by FTIR analysis. UV–visible and fluorescence spectroscopies show a blue shift towards the UV region of both absorption and band edge emission spectra respectively, and subsequently show a widening in optical band gap of anatase titania NPs, which is a consequence of band gap tuning with Co doping. These blue shifts in absorption and in emission spectra are due to the contribution of quantum size effect as well as strong Coulomb interaction effect. To conclude, the blue shifts of anatase TiO_2 NPs can make them a good candidate as a UV protector and widening of band gap is also a good sign for the application in electronic semiconductor-supported device applications. The procedure and results, presented in this paper, may provide useful guidelines for the fabrication of tunable photonic devices material.

Acknowledgements

The authors owe much to the Council of Science & Technology (CST), Government of UP, India for financial support in the form of Centre of Excellence in Materials Science (Nanomaterials). They need to express their thanks to Prof. S. S. Islam, Jamia Millia Islamia University, New Delhi for his help in FESEM with EDS measurement, and to Dr. Fauran Singh, IUAC, New Delhi for his assistance in Raman facilities. Authors are also thankful to the University Sophisticated Instrument Facility (USIF), Aligarh Muslim University, Aligarh, for providing the facility of TEM. One of the authors, Alamgir is very grateful to University Grants Commission (UGC), India for availing Maulana Azad National Fellowship [No.F.40-3(M/S)/2009(SA-III/MANF)].

References

[1] L. Li, J. Hu, W. Yang, A.P. Alivisatos, Nano Lett. 1 (2001) 349.
[2] A.P. Alivisatos, Science 271 (1996) 933.
[3] Nalwa H. Singh, Nanostructured materials and nanotechnology (2000) 257.
[4] Y. Wang, N. Herron, J. Phys. Chem. 92 (1988) 4988.
[5] L.E. Brus, J. Chem. Phys. 79 (1983) 5566.
[6] O. Legrini, E. Oliveros, A.M. Braun, Chem. Rev. 93 (1993) 671.
[7] T. Sugimoto, X. Zhou, A. Muramatsu, J. Colloid Interface Sci. 259 (2003) 43.
[8] B. O'regan, M. Gratzel, Nature 353 (1991) 737.
[9] T. Fuyuki, T. Kobayashi, H. Matsunami, J. Electrochem. Soc. 135 (1988) 248.
[10] M.R. Hoffmann, S.T. Martin, W. Choi, D.W. Bahnemann, Chem. Rev. 95 (1995) 69.
[11] U. Diebold, Surf. Sci. Rep. 48 (2003) 53.
[12] M.O. Abou-Helal, W.T. Seeber, Appl. Surf. Sci. 195 (2002) 53.
[13] R. Janisch, P. Gopal, N.A. Spaldin, J. Phys.: Condens. Matter 17 (2005) R657.
[14] S.R. Shinde, S.B. Ogale, S. Das Sarma, J.R. Simpson, H.D. Drew, S.E. Lofland, C. Lanci, J.P. Buban, N.D. Browning, V.N. Kulkarmi, J. Higgins, R.P. Sharma, R.L. Green, T. Venkatesan, Phys. Rev. B 67 (2003) 115211.
[15] T. Fukumura, Y. Yamada, H. Toyosaky, T. Hasegawa, H. Koinuma, M. Kawasaki, Appl. Surf. Sci. 223 (2004) 62.
[16] K. Wakabayashi, Y. Yamaguchi, T. Sekiya, J. Lumin. 112 (2005) 50.
[17] C. Huang, X. Liu, L. Kong, W. Lan, Q. Su, Y. Wang, Appl. Phys. A 87 (2007) 781.
[18] J.C. Yu, J.G. Yu, K.W. Ho, Z.T. Jiang, L.Z. Zhang, Chem. Mater. 14 (2002) 3808.
[19] M. Anpo, N. Aikawa, Y. Kubokawa, M. Che, C. Louis, E.J. Giamello, Phys. Chem. 89 (1985) 5017.
[20] K. Das, S.N. Sharma, M. Kumar, S.K. De, J. Phys. Chem. C 113 (2009) 14783.
[21] K. Ishikawa, K. Yoshikawa, N. Okada, Phys. Rev. B 37 (1988) 5852.
[22] B. Santara, B. Pal, P.K. Giri, J. Appl. Phys. 110 (2011) 114322.

[23] L. Yang, X. Qin, M. Gong, X. Jiang, M. Yang, X. Li, G. Li, Spectrochim. Acta Part A: Mol. Biomol. Spectros. 123 (2014) 224.
[24] V.R. Singh, K. Ishigami, V.K. Verma, G. Shibata, Y. Yamazaki, T. Kataoka, A. Fujimori, F.-H. Chang, D.-J. Huang, H.-J. Lin, C.T. Chen, Y. Yamada, T. Fukumura, M. Kawasaki, J. Appl. Phys. 100 (2012) 242404.
[25] B. Choudhury, A. Choudhury, A.K.M.M. Islam, P. Alagarsamy, M. Mukherjee, J. Magn. Magn. Mater. 323 (2011) 440.
[26] J.C. Parker, R.W. Seigel, Appl. Phys. Lett. 57 (1990) 943.
[27] D. Bersani, P.P. Lottici, X.Z. Ding, Appl. Phys. Lett. 72 (1998) 73.
[28] W.H. Ma, Z. Lu, M.S. Zhang, Appl. Phys. A 66 (1998) 621.
[29] W.F. Zhang, Y.L. He, M.S. Zhang, Z. Yin, Q. Chen, J. Phys. D: Appl. Phys. 33 (2000) 912.
[30] H.C. Choi, Y.M. Jung, S.B. Kim, Vib. Spectrosc. 37 (2005) 33.
[31] L.H. Liang, C.M. Shen, X.P. Chen, W.M. Liu, H.J. Gao, J. Phys.: Condens. Matter 16 (2004) 267.
[32] B. Choudhury, A. Choudhury, J. Appl. Phys. 114 (2013) 203906.
[33] T. Ohsaka, F. Izumi, Y. Fujiki, J. Raman Spectrosc. 7 (1978) 321.
[34] S. Sharma, S. Chaudhary, S.C. Kashyap, S.K. Sharma, J. Appl. Phys. 109 (2011) 083905.
[35] H.Y. Chuang, D.H. Chen, Nanotechnology 20 (2009) 105704.
[36] E.V. Lavrov, J. Weber, F. Borrnert, C.G. Vande Walle, R. Helbig, Phys. Rev. B 66 (2002) 165205.
[37] G. Li, L. Li, J.B. Goates, B.F. Woodfield, J. Am. Chem. Soc. 127 (2005) 8659.
[38] P. Goswami, J.N. Ganguli, Dalton Trans. 42 (2013) 14480.
[39] J.A. Wang, R. Limas-Ballesteros, T. Lopez, A. Moreno, R. Gomez, O. Novaro, X. Bokhimi, J. Phys. Chem. B 105 (2001) 9692.
[40] Timonah N. Soitah, Yang Chunhui, Sun Liang, Sci. Adv. Mater. 2 (2010) 534.
[41] M. Litter, Appl. Catal. B: Environ. 23 (1999) 89.
[42] K.M. Reddy, S.V. Manorama, A.R. Reddy, Mater. Chem. Phys. 78 (2002) 239.
[43] J.R. Simpson, H.D. Drew, S.R. Shinde, R.J. Choudhary, S.B. Ogale, T. Venkatesan, Phys. Rev. B 69 (2004) 193205.
[44] J. Xu, S. Shi, L. Li, X. Zhang, Y. Wang, X. Chen, J. Wang, L. Lv, F. Zhang, W. Zhong, J. Appl. Phys. 107 (2010) 053910.
[45] B. Choudhury, A. Choudhury, J. Luminescence 132 (2012) 178.
[46] Y. Lei, L. Zhang, G. Meng, G. Li, X. Zhang, C. Liang, W. Chen, S. Wang, Appl. Phys. Lett. 78 (2001) 1125.